

The Binary Black Hole Merger Rate from Ultraluminous X-ray Source Progenitors

Justin D. Finke^{1*} and Soebur Razzaque²

¹ *U.S. Naval Research Laboratory, Code 7653, 4555 Overlook Ave. SW, Washington, DC, 20375-5352, USA*

² *Department of Physics, University of Johannesburg, PO Box 524, Auckland Park 2006, South Africa*

31 August 2017

ABSTRACT

Ultraluminous X-ray sources (ULXs) exceed the Eddington luminosity for a $\approx 10M_{\odot}$ black hole. The recent detection of black hole mergers by the gravitational wave detector ALIGO indicates that black holes with masses $\gtrsim 10M_{\odot}$ do indeed exist. Motivated by this, we explore a scenario where ULXs consist of black holes formed by the collapse of high-mass, low-metallicity stars, and that these ULXs become binary black holes (BBHs) that eventually merge. We use empirical relations between the number of ULXs and the star formation rate and host galaxy metallicity to estimate the ULX formation rate and the BBH merger rate at all redshifts. This assumes the ULX rate is directly proportional to the star formation rate for a given metallicity, and that the black hole accretion rate is distributed as a log-normal distribution. We include an enhancement in the ULX formation rate at earlier epochs due to lower mean metallicities. With simplified assumptions, our model is able to reproduce both the rate and mass distribution of BBH mergers in the nearby universe inferred from the detection of GW 150914, LVT 151012, GW 151226, and GW 170104 by ALIGO if the peak accretion rate of ULXs is a factor $\approx 1 - 300$ greater than the Eddington rate. Our predictions of the BBH merger rate, mass distribution, and redshift evolution can be tested by ALIGO in the near future, which in turn can be used to explore connections between the ULX formation and BBH merger rates over cosmic time.

Key words: gravitational waves — X-rays: binaries — stars: black holes — stars: massive — accretion, accretion disks

1 INTRODUCTION

Ultraluminous X-ray sources (ULXs) are off-nuclear X-ray point sources in nearby galaxies with X-ray luminosities greater than the Eddington luminosity for a $\approx 10M_{\odot}$ black hole (e.g., Fabbiano 1988; Mizuno et al. 1999; Colbert & Mushotzky 1999; Colbert & Ptak 2002; Liu & Mirabel 2005). They are likely related to accretion onto high-mass black holes, although their exact nature is still in question; until recently, there was no reliable evidence for black holes with masses $\gtrsim 10 M_{\odot}$ outside of the supermassive black holes as the centers of galaxies. It has been suggested that ULXs are a result of beamed, anisotropic emission (Georganopoulos, Aharonian, & Kirk 2002; Körding, Falcke, & Markoff 2002), although strong beaming is now disfavored due to observations of ionized nebulae around some ULXs that indicates their emission is isotropic (e.g., Pakull & Mirioni 2003; Gutiérrez 2006; Bergeha et al. 2010). The two remaining possibilities are super-Eddington accretion (e.g., Begelman 2001; Poutanen et al. 2007; Finke & Böttcher 2007;

Sądowski & Narayan 2015), or accretion onto black holes with masses $\gtrsim 10M_{\odot}$, perhaps even as high as 10^4M_{\odot} , so-called intermediate-mass black holes (IMBHs; Colbert & Mushotzky 1999). Hydrodynamic simulations of stellar evolution and supernovae have indicated that such black holes could be the remnants of very high mass, very low metallicity stars (e.g., Spera, Mapelli, & Bressan 2015). Indeed, there is some low significance evidence that ULXs are preferentially found in metal-poor galaxies (Mapelli et al. 2010; Prestwich et al. 2013). Low-metallicity, Population III stars were quite common in the early universe. However, accretion from the ISM onto IMBH remnants from the first stars are unlikely to be able to explain the local ULX population (Volonteri & Perna 2005). A scenario where the IMBH is produced by the collapse of a Population III star in the early universe and then later captures a star through dynamical interactions and becomes a ULX was shown by Kuranov et al. (2007) to be incapable of explaining the ULX population. Alternatively, high-mass black holes could form through interactions in star clusters (Downing et al. 2011; Morscher et al. 2015) although in this case it is unlikely that enough ULX could be formed by black holes

* justin.finke@nrl.navy.mil

capturing high-mass stars to explain the local population (e.g., Blecha et al. 2006).

The detection of gravitational waves by the Advanced Laser Interferometer Gravitational Wave Observatory (ALIGO) has given the first evidence that black holes with masses $\gtrsim 10M_\odot$ exist. Previous mass estimates $\gtrsim 10M_\odot$ of the black hole in IC 10 X-1 (Prestwich et al. 2007; Silverman & Filippenko 2008) are no longer considered reliable (Laycock et al. 2015; Abbott et al. 2016d). The first gravitational wave event detected, dubbed GW 150914, consisted of the merging of two black holes with masses $36^{+5}_{-4}M_\odot$ and $29 \pm 4M_\odot$ merging to form a black hole with mass $62 \pm 4M_\odot$ at redshift $z = 0.09^{+0.03}_{-0.04}$ (Abbott et al. 2016d,e), although the pre-merger black hole mass estimates were later updated to $35^{+5}_{-3}M_\odot$ and $30^{+3}_{-4}M_\odot$ (Abbott et al. 2016c). More merging black holes have been subsequently detected by ALIGO (Abbott et al. 2016b,a, 2017). In this paper, we re-evaluate the nature of ULXs in light of these discoveries. We investigate a scenario for ULX formation similar to that proposed by Zampieri & Roberts (2009), that ULXs include high-mass black holes formed by low-metallicity stars local to the ULX (i.e., not from stars in the early universe). In our scenario, the ULXs are born as binary high-mass field stars, before one of the stars explodes in a supernova and turn into a black hole. Thus, the black hole in a ULX system is born not long before the ULX system was created. The extremely high mass stars needed to make the high-mass black holes do indeed exist in the local universe; the η Carina system consists of binary stars whose masses combine to be $250M_\odot$ (Kashi & Soker 2010). The fact that most high mass stars are found in binaries (García & Mermilliod 2001; Sana et al. 2008) would also seem to make this scenario likely.

In Section 2, we develop a simple model for ULXs and compute the ULX formation rate as a function of redshift. Inoue, Tanaka, & Isobe (2016) have suggested that ULXs are the progenitors of BBH mergers; that is, an accreting high-mass black hole and high-mass star become a binary black hole (BBH) system after the companion star explodes in a supernova; and the BBH eventually merges, and is potentially detectable by ALIGO (see also Bulik et al. 2011). They use this to estimate the rate of BBH mergers expected in the local universe. In Section 3 we use our knowledge of the ULX formation rate to estimate the BBH merger rate. Our calculation goes beyond the estimates by Inoue et al. (2016) and explores detailed redshift and metallicity dependences of the ULX and corresponding BBH merger rates for different binary BH mass combinations. Our modeling results are compared with the rate and mass distribution inferred from mergers that have been detected so far (GW 150914, LVT 151012, GW 151226, and GW 170104; Abbott et al. 2016a, 2017). Finally, we conclude with a discussion (Section 4). In Appendix A we compute an enhancement in cosmological ULX production due to decreasing metallicity at higher redshifts.

2 ULX FORMATION

In this section, we discuss our simple ULX model, and its formation rate, both in the local universe and extending to high redshift. We consider only those ULXs that are compact objects with high-mass companions, neglecting those with low-mass companions, which cannot become BBH systems. We make a number of simplifying assumptions about the evolution of high mass stars, binaries, and supernovae. We avoid discussion of poorly-understood tidal chemical mixing (e.g., Mandel & de Mink 2016;

de Mink & Mandel 2016) and common envelope binary evolution (e.g., Belczynski et al. 2007, 2016).

2.1 Simple ULX Model

Consider two massive ($\gtrsim 10M_\odot$), low-metallicity stars. After some time, one of the stars explodes in a supernova leaving a neutron star or black hole remnant of mass $M_{\text{BH},1}$. At some point in the binary's life time, the black hole is accreting from its companion star, creating intense X-ray radiation with an X-ray luminosity $L_X \geq 10^{39} \text{ erg s}^{-1}$. The binary is in its ULX phase. The X-ray luminosity of the ULX can be expressed as a fraction ℓ_{Edd} of the Eddington luminosity, so that

$$L_X = \ell_{\text{Edd}} L_{\text{Edd}} = \ell_{\text{Edd}} L_0 m_{\text{BH},1}, \quad (1)$$

where $L_0 = 1.26 \times 10^{38} \text{ erg s}^{-1}$ and $m_{\text{BH},1} = M_{\text{BH},1}/M_\odot$. We assume that the ULX emission is isotropic, consistent with observations of ionized nebulae around some ULXs. We take the ULX lifetime to be $t_{\text{ULX}} = 0.1 \text{ Myr}$, consistent with several recent estimates (see the discussion by Mineo et al. 2012; Inoue et al. 2016). However, this value is uncertain, as discussed in Section 4.

Eventually, the massive companion star will exhaust its nuclear fuel and also end its life in a supernova that leaves behind a compact object of mass $M_{\text{BH},2}$. We assume that $M_{\text{BH},2} \leq M_{\text{BH},1}$ since generally lower mass stars live longer and make lower mass compact objects than higher mass stars when in isolation, although this can be altered in the mass exchange in binary systems. We allow $m_{\text{BH},1} = M_{\text{BH},1}/M_\odot$ and $m_{\text{BH},2} = M_{\text{BH},2}/M_\odot$ to go down to 1.4, we actually are including neutron stars as well, since some ULXs are known to be accreting neutron stars (e.g., Bachetti et al. 2014; Israel et al. 2017a,b). However, we will refer to them as black holes for most of this paper, since in our model black hole ULXs will outnumber neutron star ULXs, consistent with population synthesis modeling (Fragos et al. 2015), although if ULXs are anisotropic emitters, this may not be the case (Wiktorowicz et al. 2017; Middleton & King 2017). For the maximum mass of the compact object, we use $m_{\text{BH,max}} = 130$ based on the maximum possible black hole mass found from stellar evolution and supernova models of low-metallicity stars by Spera et al. (2015).

2.2 Local ULX Formation

We are interested in ULXs that eventually become BBHs, so these must be ULXs with high-mass stellar companions. There is evidence that most ULXs in spiral galaxies have high-mass companions, while ULXs in elliptical galaxies have low-mass companions (e.g., Swartz et al. 2004). We assume that all ULXs in spiral galaxies have high-mass companions, and all ULXs in elliptical galaxies have low-mass companions, so that we only explore those ULXs that are found in spiral galaxies (similar to Inoue et al. 2016). In a survey of nearby galaxies, Walton et al. (2011) found that the X-ray luminosity function for ULXs in spiral galaxies is

$$N_X(L_X) = \frac{dN}{dL_X} \propto L_X^{-\alpha} \quad (2)$$

with $\alpha = 1.85 \pm 0.11$ and L_X ranging from $L_{\text{min}} = 10^{39} \text{ erg s}^{-1}$ to $L_{\text{max}} = 6 \times 10^{40} \text{ erg s}^{-1}$. Similarly, they find the number of ULXs per unit stellar mass of the spiral host galaxy is

$$N_X(M_{\text{Gal}}) = \frac{dN}{dM_{\text{Gal}}} = N_0 M_3^{-\beta} \quad (3)$$

where $M_{Gal} = 10^3 M_3 MM_\odot$ is the host galaxy stellar mass¹, $\beta = 0.64 \pm 0.07$, and

$$N_0 = N_X(M_3 = 1) = 3.3 \times 10^{-4} MM_\odot^{-1}. \quad (4)$$

If the Milky Way has a stellar mass of $(6.43 \pm 0.63) \times 10^4 MM_\odot$ (McMillan 2011) then Equation (3) predicts ≈ 1.5 ULXs in our Galaxy, approximately consistent with 0 that are observed. Combining Equations (2) and (3) we expect that

$$N_X(L_X, M_{Gal}) = \frac{dN}{dL_X dM_{Gal}} = N'_0 M_3^{-\beta} L_{40}^{-\alpha}, \quad (5)$$

where $L_{40} = L_X / (10^{40} \text{ erg s}^{-1})$ and $N'_0 = N_X(L_{40} = 1, M_3 = 1)$. Here we assume that $N_X(L_X)$ and $N_X(M_{Gal})$ are independent. Using

$$N_X(M_{Gal}) = \int_{L_{\min}}^{L_{\max}} dL N_X(L_X, M_{Gal}) \quad (6)$$

one can solve for the normalization constant in Equation (5),

$$N'_0 = 2.4 \times 10^{-5} MM_\odot^{-1} (10^{40} \text{ erg s}^{-1})^{-1}. \quad (7)$$

The ULX formation rate as a function of L_X and host galaxy mass can be estimated as

$$\begin{aligned} \dot{N}_X(L_X, M_{Gal}) &= \frac{dN}{dt dL_X dM_{Gal}} \\ &= \frac{N_X(M_{Gal}, L_X)}{t_{\text{ULX}}}. \end{aligned} \quad (8)$$

The cosmological ULX formation rate per unit comoving volume, per unit X-ray luminosity, in the local universe can be found by convolving $\dot{N}_X(L_X, M_{Gal})$ with the spiral galaxy mass function in the local universe, $\phi(M_{Gal}; z = 0) = dN/(d(\log_{10} M_{Gal})dV)$, so that

$$\begin{aligned} \dot{n}_X(L_X; z = 0) &= \frac{dN}{dV dt dL_X} \\ &= \int_{M_{Gal, \min}}^{M_{Gal, \max}} dM_{Gal} \\ &\times \frac{\phi(M_{Gal}; z = 0)}{\ln(10)} \\ &\times \dot{N}_X(L_X, M_{Gal}) \end{aligned} \quad (9)$$

where we use $M_{Gal, \min} = 10^2 MM_\odot$ and $M_{Gal, \max} = 10^7 MM_\odot$. The function $\phi(M_{Gal}; z = 0)$ was found by Moffett et al. (2016), which they represented by a Schechter function,

$$\begin{aligned} \phi(M_{Gal}; z = 0) &= \phi^* \ln(10) \left(\frac{M_{Gal}}{M^*} \right)^{1+\delta} \\ &\times \exp\left(-\frac{M_{Gal}}{M^*}\right). \end{aligned} \quad (10)$$

They found it was well-fit with parameters $\phi^* = (8.55 \pm 1.00) \times 10^{-4} \text{ Mpc}^{-3}$, $\delta = -1.39 \pm 0.02$, and $M^* = 10^{10.70 \pm 0.05} M_\odot$, which we use. The total ULX formation rate density for all ULXs can be found by integrating,

$$\dot{n}_{X, \text{tot}}(z = 0) = \int_{L_{\min}}^{L_{\max}} dL_X \dot{n}_X(L_X; z = 0). \quad (11)$$

¹ $MM_\odot = 10^6 M_\odot$

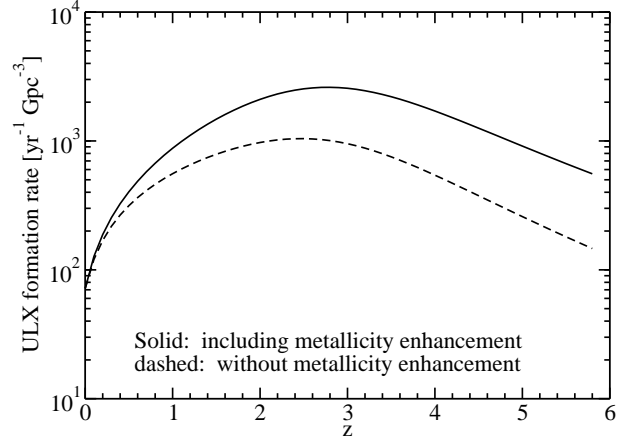


Figure 1. Total ULX formation rate density $\dot{n}_{X, \text{tot}}(z)$ computed from Equation (13), with and without the metallicity enhancement factor, $\zeta(z)$.

2.3 Cosmological ULX Formation

There is evidence that high-mass X-ray binaries are connected with star formation (e.g., Grimm et al. 2003; Ranalli et al. 2003). Since in our model ULXs are formed from short-lived, high mass stars, the ULX formation rate should follow the star formation rate. However, in our model ULXs are formed from low-metallicity stars, and the average metallicity decreases with redshift. There is in fact some weak evidence that lower metallicity galaxies host more ULXs for a given star formation rate (e.g., Mapelli et al. 2010; Prestwich et al. 2013). In Appendix A we use some of this evidence to estimate a metallicity enhancement in ULX formation, $\zeta(z)$.

Using the knowledge of the SFR, metallicity enhancement, and local ULX formation rate as found in Section 2.2, one can find the ULX formation rate density for any z ,

$$\dot{n}_X(L_X; z) = \frac{\psi(z)}{\psi(z = 0)} \zeta(z) \dot{n}_X(L_X; z = 0), \quad (12)$$

where $\psi(z) = dM_*/(dV dt)$ is the star formation rate (SFR) density. Finke, Razzaque, & Dermer (2010) found that the combination of the Cole et al. (2001) SFR, with parameters found by Hopkins & Beacom (2006), combined with an initial mass function (IMF) from Baldry & Glazebrook (2003), reproduced the luminosity density data available at the time better than other combinations of SFR and IMF. Therefore, we use this $\psi(z)$ here.

The total ULX formation rate density for all ULXs can be found by integrating,

$$\dot{n}_{X, \text{tot}}(z) = \int_{L_{\min}}^{L_{\max}} dL_X \dot{n}_X(L_X; z), \quad (13)$$

where recall $L_{\min} = 10^{39} \text{ erg s}^{-1}$ to $L_{\max} = 6 \times 10^{40} \text{ erg s}^{-1}$. This result is shown in Figure 1, with and without the metallicity enhancement factor (i.e., the latter has $\zeta(z) = 1$). Not surprisingly, the ULX formation rate follows the shape of the star formation rate without the metallicity enhancement; including the enhancement, the ULX formation rate is larger at higher redshifts.

3 BBH MERGERS

3.1 Model

After the companion star ends its life in a supernova, and joins its companion as a black hole, the BBH system is created. Thus far, we have made no assumptions about the Eddington ratio of the ULX. However, to use the ULX formation rate to estimate the BBH merger rate, we must use a distribution of Eddington ratios to convert from the ULX X-ray luminosities to the BBH masses. A study of accreting stellar-mass black holes indicates that this distribution resembles a log-normal distribution,

$$P_\ell(\ell_{\text{Edd}}) = \frac{A_\ell}{\ell_{\text{Edd}}} \times \exp\left\{\frac{-[\ln(\ell_{\text{Edd}}) - \ln(\ell_{\text{Edd,pk}})]^2 - \sigma^2}{2\sigma^2}\right\}, \quad (14)$$

with peak $\ell_{\text{Edd,pk}} \approx 10^{-2.5} - 10^{-2}$ and $\sigma \approx 1$ (Reynolds & Miller 2013). A study of X-ray selected broad-line active galactic nuclei by Suh et al. (2015) found the Eddington ratios of these objects are distributed as a log-normal distribution, with $\ell_{\text{Edd,pk}} = 10^{-0.6}$ and $\sigma = 0.8$. If the accretion flow of ULXs behaves similarly to accreting stellar-mass black holes and active galactic nuclei, it seems reasonable to assume that this distribution of ℓ_{Edd} for ULXs is also a log-normal distribution. Here we will use a log-normal distribution for $P_\ell(\ell_{\text{Edd}})$ with $\sigma = 1$ and various values for $\ell_{\text{Edd,pk}}$, which we consider a free parameter. Since we have $L_{\text{max}} = 6 \times 10^{40} \text{ erg s}^{-1}$, and the maximum possible black hole mass was found to be $130M_\odot$ by Spera et al. (2015), the Eddington ratio must extend to at least $\ell_{\text{Edd}} > 3.7$. Thus, we will allow the value of ℓ_{Edd} to be > 1 to explain the brightest ULXs, although the log-normal distribution may be more questionable for ULXs with $\ell_{\text{Edd}} \gg 1$, since the distribution was found for objects with lower ℓ_{Edd} . In equation (14), the normalization constant is found by performing the integral

$$1 = \int_{\ell_{\text{min}}}^{\ell_{\text{max}}} d\ell_{\text{Edd}} P_\ell(\ell_{\text{Edd}}) \quad (15)$$

and solving for A_ℓ , where $\ell_{\text{min}} = L_{\text{min}}/(L_0 m_{\text{BH},1})$ and $\ell_{\text{max}} = L_{\text{max}}/(L_0 m_{\text{BH},1})$.

The BBHs' orbits decay by emitting gravitational waves, and they merge after

$$t_{\text{GW}} = 5.6 \times 10^7 \left(\frac{a}{10R_\odot}\right)^4 \left(\frac{M_{\text{BH},1}}{30M_\odot}\right)^{-1} \times \left(\frac{M_{\text{BH},2}}{30M_\odot}\right)^{-1} \left(\frac{M_{\text{BH},1}}{30M_\odot} + \frac{M_{\text{BH},2}}{30M_\odot}\right)^{-1} \text{ yr} \quad (16)$$

(Peters 1964) where a is the initial separation of the BBHs. If a binary black hole system is created at redshift z_X and merges at z_m , then

$$t_{\text{GW}} = \int_{z_m}^{z_X} dz \left| \frac{dt}{dz} \right| \quad (17)$$

where

$$-\frac{dt}{dz} = \frac{1}{H_0(1+z)\sqrt{(1+z)^3\Omega_m + \Omega_\Lambda}} \quad (18)$$

in a flat Λ CDM universe. To find z_X for a given z_m , $m_{\text{BH},1}$, $m_{\text{BH},2}$, and a , we solve Equations (16) and (17) numerically using standard cosmological parameters $H_0 = 70 \text{ km s}^{-1} \text{ Mpc}^{-1}$, $\Omega_m = 0.3$, and $\Omega_\Lambda = 0.7$. Doing this requires knowledge of the distributions of $m_{\text{BH},2}$, and a .

Abbott et al. (2016a) use a power-law distribution for $m_{\text{BH},2}$ and we follow their calculation, so that the distribution, normalized to unity, is

$$P_m(m_{\text{BH},2}) = A_m m_{\text{BH},2}^\gamma \quad (19)$$

where

$$A_m = \begin{cases} (\gamma + 1)/(m_{\text{BH},1}^{\gamma+1} - m_{\text{BH,min}}^{\gamma+1}) & \gamma \neq 1 \\ 1/\ln(m_{\text{BH},1}/m_{\text{BH,min}}) & \gamma = 1 \end{cases}. \quad (20)$$

Abbott et al. (2016a) use $\gamma = 0$, and consequently so do we, although γ is in principle a free parameter.

The separation of binaries can change during their lives due to mass exchange between the two stars due to Roche lobe overflow and winds, tidal interactions, magnetic braking, and emission of gravitational radiation. Further, when massive stars explode the resulting compact object can get a significant ‘‘kick’’, which can substantially alter the binary separation. These processes are modeled in detail in sophisticated population synthesis codes (e.g., Hurley et al. 2002; Belczynski et al. 2002, 2008). For our purposes, we are only interested in the separation when binaries become BBHs. Population synthesis calculations by Belczynski et al. (2002) indicate that the initial separation of the BBHs is a distribution with a peak of about $a = 10R_\odot$ in their ‘‘standard model’’. Therefore, we use a log-normal distribution for the initial separation of the BBHs, normalized to unity over $a = 0$ to $a = \infty$,

$$P_a(a) = \frac{1}{\sigma_a a \sqrt{2\pi}} \times \exp\left\{\frac{-[\ln(a) - \ln(a_{\text{pk}}) - \sigma_a^2]^2}{2\sigma_a^2}\right\}, \quad (21)$$

with peak $a_{\text{pk}} = 10R_\odot$ and $\sigma_a = 0.6$. In general, however, a_{pk} can be considered another free parameter.

Putting everything together, the merger rate density

$$\begin{aligned} \dot{n}_m(m_{\text{BH},1}; z_m) &= \frac{dN}{dV dt dm_{\text{BH},1}} \\ &= \left\{ \int_{\ell_{\text{min}}}^{\ell_{\text{max}}} d\ell_{\text{Edd}} P_\ell(\ell_{\text{Edd}}) \right. \\ &\quad \times \left. \frac{L_X}{m_{\text{BH},1}} \dot{n}_X(L_X; z = 0) \right\} \\ &\quad \times \int_{m_{\text{BH,min}}}^{m_{\text{BH},1}} dm_{\text{BH},2} P_m(m_{\text{BH},2}) \\ &\quad \times \int_0^\infty da P_a(a) \\ &\quad \times \frac{\psi(z_X(z_m, m_{\text{BH},1}, m_{\text{BH},2}, a))}{\psi(z = 0)} \\ &\quad \times \zeta(z_X(z_m, m_{\text{BH},1}, m_{\text{BH},2}, a)), \end{aligned} \quad (22)$$

where $\ell_{\text{min}} = L_{\text{min}}/(L_0 m_{\text{BH},1})$, $\ell_{\text{max}} = L_{\text{max}}/(L_0 m_{\text{BH},1})$, L_X/m_{BH} and dL_X/dm_{BH} are calculated from Equation (1), and $\dot{n}_X(L_X; z = 0)$ is given by Equation (9). The total merger rate

$$\dot{n}_{m,\text{tot}}(z_m) = \int_{m_{\text{BH,min}}}^{m_{\text{BH,max}}} dm \dot{n}_m(m; z_m), \quad (23)$$

where recall $m_{\text{BH,min}} = 1.4$ and $m_{\text{BH,max}} = 130$.

The total merger rate is plotted in Figure 2, again, with and without the metallicity enhancement factor $\zeta(z)$. The overall shape of the curves roughly follows the ULX formation rate, delayed by a time t_{GW} . The lower the Eddington ratio $\ell_{\text{Edd,pk}}$, the more BBH

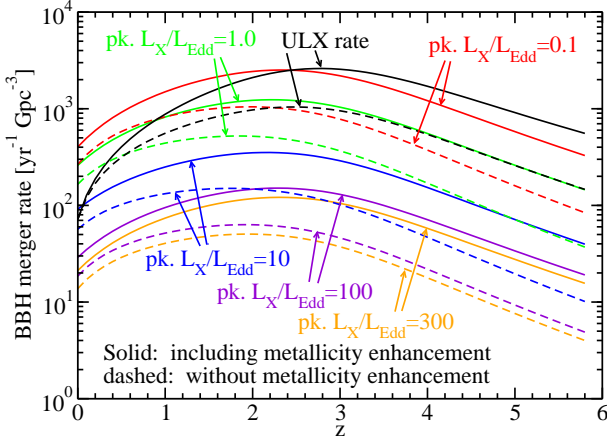


Figure 2. Total BBH merger rate density, $\dot{n}_{m,tot}(z_m)$, computed from Equation (23), with and without the metallicity enhancement factor, $\zeta(z)$. Different values of the peak Eddington ratio, $\ell_{Edd,pk}$, were used, as indicated on the plot. The ULX formation rate, as in Figure 1, is also shown as indicated.

mergers will originate from the observed ULX progenitor population.

The BBH merger rate per unit logarithmic primary black hole mass bin, $m_{BH,1} \times \dot{n}_m(m_{BH,1}; z_m)$, for $\ell_{Edd,pk} = 10$ is plotted as a function of $M_{BH,1}$ for various values of z_m in Figure 3. At low values of $M_{BH,1}$ mergers are fewer, since there is not enough time for many of them to occur within the age of the universe. At higher redshifts, low-mass mergers become fewer in number, since the universe is younger and there is less time for mergers to occur. Thus, overall the peak increases at high z . This means this model produces few binary neutron star systems such as PSR 1913+16 (Taylor, Fowler, & McCulloch 1979) and PSR J0737–3039 (Burgay et al. 2003) that will merge within the age of the universe. However, we note that the population synthesis calculations of Belczynski et al. (2002) find a separate peak at $a = 0.3R_\odot$ for the initial separation of binary neutron stars. So another population, which will not go through a ULX phase, can explain the binary neutron stars. Also note the overall normalization increases up to $z \approx 3$ and decreases at higher z , in agreement with Figure 2. In Figure 4 $m_{BH,1} \times \dot{n}_m(m_{BH,1}; z_m = 0)$ is plotted as a function of $m_{BH,1}$ and $m_{BH,2}$. This was computed from Equation (22) using $P_m(m_{BH,2}) \rightarrow \delta(m_{BH,2} - m'_{BH,2})$. The peak in merger rate is where $m_{BH,1} = m_{BH,2} \approx 6$, in agreement with Figure 3.

The BBH merger rate per unit logarithmic primary black hole mass bin at $z_m = 0$ as a function of $m_{BH,1}$ is plotted in Figure 5 for different values of the peak initial BBH separation a_{pk} , instead of our “default” value $a_{pk} = 10R_\odot$. Clearly, both the low-mass cutoff, and peak are strongly dependent on a_{pk} . This leads us to the conclusion that future observations of mergers by ALIGO could build up enough statistics to observe this enhancement, which would then constrain the initial BBH separation.

The cumulative merger rate as measured by the observer can be found from

$$\dot{N}_{m,tot}(< z) = 4\pi \int_0^z dz_m \frac{\dot{n}_{m,tot}(z_m)}{1+z} \frac{dV_c}{dz_m} \quad (24)$$

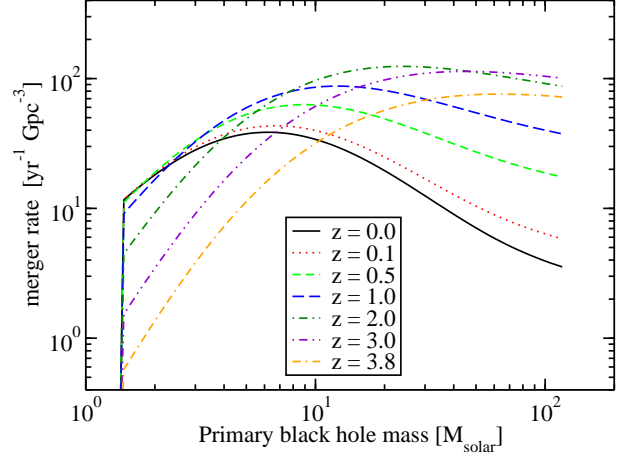


Figure 3. BBH merger rate density per unit logarithmic primary black hole mass bin, $m_{BH,1} \times \dot{n}_m(m_{BH,1}; z_m)$, plotted as a function of primary black hole mass, $m_{BH,1}$, for various values of z_m . This calculation uses $\ell_{Edd,pk} = 10$ and includes the metallicity enhancement factor.

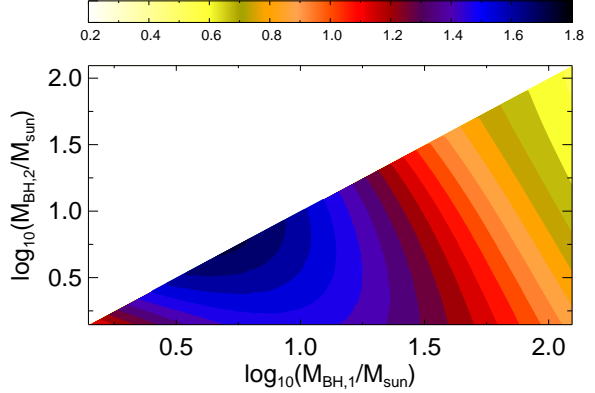


Figure 4. BBH merger rate density per unit logarithmic black hole mass bin plotted as a function of $m_{BH,1}$ and $m_{BH,2}$, for $z_m = 0$. This calculation uses $\ell_{Edd,pk} = 10$ and includes the metallicity enhancement factor. The contours show $\log_{10}[m_{BH,1} \dot{n}_m(m_{BH,1}; z_m = 0)] / (\text{yr}^{-1} \text{Gpc}^{-3})$ as indicated by the bar.

where

$$\frac{dV_c}{dz} = \frac{c d_c(z)^2}{H_0 \sqrt{(1+z)^3 \Omega_m + \Omega_\Lambda}}, \quad (25)$$

and

$$d_c(z) = \frac{c}{H_0} \int_0^z \frac{dz'}{\sqrt{(1+z')^3 \Omega_m + \Omega_\Lambda}} \quad (26)$$

is the comoving distance. This is plotted in Figure 6 for models that include our metallicity enhancement factor. The cumulative BBH merger rate follows the same basic pattern as the merger rate (Fig. 2), with lower $\ell_{Edd,pk}$ models having higher merger rates. The cumulative merger rate for up to $z = 1$, approximately the limiting redshift of ALIGO when it reaches its design sensitivity, as a function of $m_{BH,1}$ and $m_{BH,2}$ is shown in Figure 7. This was again

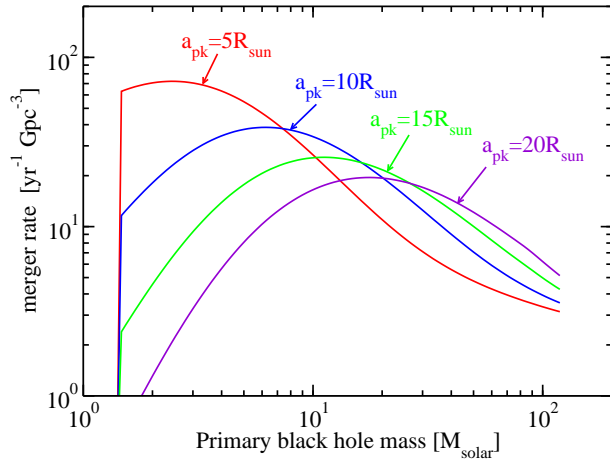


Figure 5. BBH merger rate density per unit logarithmic primary black hole mass bin, $m_{\text{BH},1} \times \dot{n}_m(m_{\text{BH},1}; z_m = 0)$, plotted as a function of primary black hole mass, $M_{\text{BH},1}$, for $\ell_{\text{Edd,pk}} = 10$, plotted for various values of the initial BBH merger separation, a , as indicated on the plot. This calculation includes the metallicity enhancement factor.

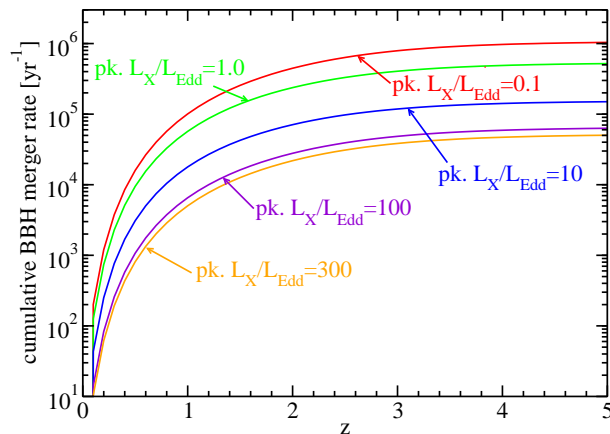


Figure 6. Cumulative BBH merger rate density, $\dot{N}_{m,tot}(< z)$, computed from Equation (24), including the metallicity enhancement factor.

calculated with $P_m(m_{\text{BH},2}) \rightarrow \delta(m_{\text{BH},2} - m'_{\text{BH},2})$. Mergers are expected to be maximized at $m_{\text{BH},1} \approx m_{\text{BH},2} \approx 6$.

3.2 Comparison with Other BBH Merger Models

Inoue et al. (2016) also used ULXs to estimate the merger rate in the local universe. Our calculations generally predict a merger rate greater than theirs (see their Figures 1 and 2). This is despite the fact that our luminosity function is actually slightly lower than the one they use by a factor of 2, below the exponential cutoff they use at high L_X . This is due to our taking into account the changing star formation rate, which is greater at higher z .

Our merger rate estimation can also be compared with the calculations by Mandel & de Mink (2016). Those authors simulated

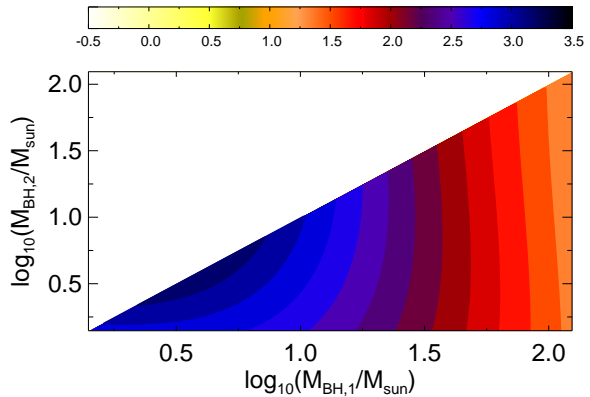


Figure 7. Cumulative BBH merger rate for $z < 1$, plotted as a function of $M_{\text{BH},1}$ and $M_{\text{BH},2}$. This calculation uses $\ell_{\text{Edd,pk}} = 10$ and includes the metallicity enhancement factor. The contours show $\log_{10}[\dot{N}_{m,tot}(z < 1)]/(\text{yr}^{-1})$ as indicated by the bar.

the formation of BBH systems from chemically homogeneous evolution of closely-interacting massive binary stars. All our models shown in Figure 2 are above theirs. The evolution at higher redshift is quite different. Mandel & de Mink (2016) find a peak of $\approx 20 \text{ Gpc}^{-3} \text{ yr}^{-1}$ at $z \approx 0.5$, then a merger rate declining sharply after that, so that there are hardly any mergers above $z = 1.5$; see their Figure 7.

By contrast, estimates by Dominik et al. (2013) find large numbers of BBH mergers ($\gtrsim 10 - 100 \text{ yr}^{-1} \text{ Gpc}^{-3}$) out to redshift $z \approx 16$, mainly depending on whether or not they include “high kicks”. Their “high kick” scenario seems to be ruled out by rate inferred by the detection of BBH mergers by ALIGO, since this scenario predicts $\lesssim 1 \text{ yr}^{-1} \text{ Gpc}^{-3}$ at low z . In their scenarios without high kicks, they find $10 - 100 \text{ yr}^{-1} \text{ Gpc}^{-3}$ at $z = 0$, consistent with our models with $\ell_{\text{Edd,pk}} \gtrsim 1.0$. Their results for the evolution of the merger rate at high z is also different from ours; while our merger rates peak at $z = 2 - 3$, in all of their scenarios the merger rate peaks at $z \gtrsim 4$.

The predictions for the evolution of BBH merger rate with z by Mandel & de Mink (2016) and Dominik et al. (2013) not only differ substantially from our predictions, but differ substantially from each other as well. Both these authors take a more “first principles” approach, while our calculation is more empirically-motivated. We hope this makes it more accurate, although we note that there are many unknowns in our calculation (discussed further in Section 4). ALIGO will be able to detect BBH mergers out to no higher than $z \approx 1$ when it reaches its peak sensitivity in ~ 2020 (Abbott et al. 2016d); the differences in the merger rate predictions by ourselves, Mandel & de Mink (2016), and Dominik et al. (2013) at higher z are unlikely to be observed in the near future. However, the striking rapid evolution in the merger rate with z predicted by Mandel & de Mink (2016) at $z < 1$ should be confirmed or refuted with further ALIGO observations.

3.3 Comparison with ALIGO Observations

Based on the ALIGO detection of three BBH mergers: GW 150914, GW 151226, the lower significance LVT 151012, Abbott et al. (2016a) constrained the BBH merger rate to be between 9 and $240 \text{ Gpc}^{-3} \text{ yr}^{-1}$ in the local universe, with the most likely value

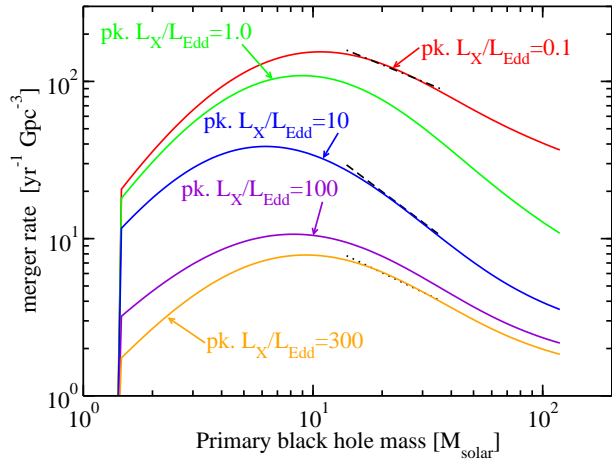


Figure 8. BBH merger rate density, $m_{\text{BH},1} \times \dot{n}_m(m_{\text{BH},1}; z_m = 0)$, plotted as a function of primary black hole mass, $m_{\text{BH},1}$, for various values of the median Eddington ratio, ℓ_{Edd} , as indicated on the plot. The black dashed, dotted, and dashed-dotted lines show power-laws, $\dot{n}_m(m_{\text{BH},1}; z_m) \propto m_{\text{BH},1}^{-2.1}$, $\propto m_{\text{BH},1}^{-1.7}$, and $\propto m_{\text{BH},1}^{-1.6}$, respectively, between $m_{\text{BH},1} = 14$ and $m_{\text{BH},1} = 36$, the range of primary black hole masses observed by ALIGO.

being $\approx 70 \text{ Gpc}^{-3} \text{ yr}^{-1}$ with an event-based analysis, and $\approx 100 \text{ Gpc}^{-3} \text{ yr}^{-1}$ with a power-law fit to the distribution of $m_{\text{BH},1}$ (more on this below). The additional detection of GW 170104 tightens this range a bit, to 12–213 $\text{Gpc}^{-3} \text{ yr}^{-1}$ (Abbott et al. 2017). All of our model curves in Figure 2 consistent with $\ell_{\text{Edd,pk}} > 1.0$ are within this range, with the closest model being the one with $\ell_{\text{Edd,pk}} = 10$. We conclude, based on the inferred ALIGO merger rate, that our model is a good representation if $\ell_{\text{Edd,pk}} \gtrsim 1.0$ for ULXs.

From ALIGO detections of BBH mergers, one can infer more information than just the total merger rate. Based on detections in ALIGO’s first observing run, and assuming that $\dot{n}_m(m_{\text{BH},1}; z_m \approx 0) \propto m_{\text{BH},1}^{-\theta}$, Abbott et al. (2016a) infer $\theta = 2.5_{-1.6}^{+1.5}$, for mergers with $m_{\text{BH},1}$ between $14.2_{-3.7}^{+8.3}$ (GW 151226) and $36.2_{-3.8}^{+5.2}$ (GW 150914). With the addition of GW 170104, this was revised to $\theta = 2.3_{-1.4}^{+1.3}$. In our model, on a plot of the merger rate as a function of $m_{\text{BH},1}$, the slope is weakly dependent on $\ell_{\text{Edd,pk}}$, as Figure 8 demonstrates. Here we also plot various power-laws consistent with the inferred ALIGO distribution for $14 < m_{\text{BH},1} < 36$. The mass distributions for all of our models shown in Figure 8 are consistent with the ALIGO observations, which have admittedly large error bars. Our model is thus fairly robust with respect to the free parameter $\ell_{\text{Edd,pk}}$, and we conclude that our model with $\ell_{\text{Edd,pk}} \approx 1 - 300$ can reproduce both the inferred rate and mass distribution of BBH mergers.

4 DISCUSSION

We have explored the scenario where ULXs consist of a massive black hole and companion star, become BBH systems, where the BBHs finally merge and create gravitational waves potentially detectable by ALIGO. By assuming that the ULX formation rate is directly proportional to the star formation rate (modulo metallicity

effects that are taken into account as described in Appendix A), we computed the ULX formation rate as a function of redshift. We then assumed that every ULX becomes a BBH, and took into account the time for a BBH merger to occur, to compute the BBH merger rate. As discussed in Section 2, we made a number of simplifying assumptions about the evolution of high mass stars, binaries, and supernovae. For instance, Dominik et al. (2013) have a fairly large suite of compact object merger rate models with various assumptions about whether Hertzsprung Gap stars can be common-envelope donor stars, whether or not delayed supernovae occur, and other variations.

Our derivation of the metallicity enhancement factor (Appendix A) makes use of a number of tentative results: namely, the relation between the metallicity of a host galaxy and the enhancement in the number of ULXs it produces, and in the evolution of the average metallicity of galaxies with redshift. For the latter, we note that a similar correlation from Kewley & Kobulnicky (2005, 2007) was used by Mandel & de Mink (2016); and it is very similar to the “high-end” metallicity evolution used by Dominik et al. (2013). Further studies on the relationship of the number of ULXs and host galaxy metallicity, and the evolution of metallicity in the universe, could greatly improve our estimates.

We find that our model is consistent with the rate and distribution of BBH mergers inferred from the ALIGO detections if $\ell_{\text{Edd,pk}} = 1 - 300$. Our scenario requires super-Eddington accretion on to black holes with masses $\leq 130M_{\odot}$. This means that if our model is accurate and the BBH mergers observed by ALIGO originated as ULXs, a large fraction, possibly even the great majority, of ULXs have super-Eddington accretion. There is evidence for super-Eddington accretion in some ULXs; for example the discovery of pulsar ULXs requires super-Eddington accretion (Bachetti et al. 2014; Fürst et al. 2016; Israel et al. 2017a,b). The X-ray spectrum of a ULX in NGC 5907 in various states led Walton et al. (2015) to conclude that this source was accreting at a super-Eddington rate. ALIGO could see 100s of BBH mergers in the near future (e.g., de Mink & Mandel 2016). As it detects more mergers, the large errors on the inferred rate and distribution will get smaller, and our model parameters, such as $\ell_{\text{Edd,pk}}$ and a_{pk} could be constrained.

One major unknown is the ULX timescale, t_{ULX} . We use the value $t_{\text{ULX}} = 0.1 \text{ Myr}$ for all ULXs, the value used by Mineo et al. (2012) and Inoue et al. (2016). This value is consistent with the thermal timescale of high-mass main sequence stars. King et al. (2001) considered the thermal timescale to be the most likely relevant timescale for the lifetime of a ULX. However, the companion stars of ULXs may not be main sequence stars; indeed 11/62 ULXs examined by Heida et al. (2014) show infrared excesses consistent with being red supergiants; spectroscopic follow-up for one of these indicates it is indeed a red supergiant (Heida et al. 2015). Red supergiants have considerably shorter thermal timescales, and thus ULXs with red supergiant companions would have considerably shorter lifetimes. If all sources had shorter t_{ULX} , our predicted merger rate would be lower for a given $\ell_{\text{Edd,pk}}$, and higher $\ell_{\text{Edd,pk}}$ would be required to be consistent with the observed BBH merger rate from ALIGO. However, most high-mass X-ray binaries do not have supergiant companions, and if this is also true for ULXs with high mass companions (the only ones we are interested in here), on average ULXs would have $t_{\text{ULX}} \sim 0.1 \text{ Myr}$ (Mineo et al. 2012), thus we use this value. If the nuclear burning timescale is the relevant timescale for the lifetime of a ULX, the timescale could be as long as $t_{\text{ULX}} = 1 \text{ Myr}$ (Patruno & Zampieri 2008). There is some evidence for these longer t_{ULX} from the kinematics of the

nebula around the ULX NGC 1313 X-2 (Pakull & Mirioni 2002). These longer lifetimes are consistent with the ages of the star clusters where ULXs reside, which have been constrained to be $\lesssim 4\text{--}20$ Myr (Ramsey et al. 2006; Gris e et al. 2011; Poutanen et al. 2013). If we had used a larger lifetime, $t_{\text{ULX}} = 1$ Myr, lower values of $\ell_{\text{Edd,pk}}$ would be consistent with the ALIGO constraints on the merger rate.

If a large fraction of ULXs are neutron stars, their X-ray emission could be beamed. This could alter our results; see e.g., King et al. (2001); Wiktorowicz et al. (2017), King et al. (2017); or Middleton & King (2017) for an exploration of this possibility. If beaming decreased the actual luminosity a fraction b relative to the observed luminosity, there would be a factor $1/b$ more sources that are not seen. Thus, the actual number of ULXs would be a factor $1/b$ higher. If b is inversely proportional to accretion rate or intrinsic X-ray luminosity (see e.g. King 2009) then naturally the enhancement would be greater for brighter sources. The effect of a $b < 1$ on the total BBH merger rate is less obvious, but we expect it would alter the distribution of masses (e.g., Fig. 3) so that there would be more low-mass mergers and fewer high-mass mergers. Israel et al. (2017a) found that a beaming factor $b \approx 1/7$ for the neutron star ULX in NGC 5907 is consistent with expectations for a thin disk and avoidance of the ‘‘propeller’’ mechanism.

It is possible that BBHs occur from dynamical interactions in star clusters, and that this channel dominates the BBH merger rate (e.g., Sadowski et al. 2008; O’Leary et al. 2016; Chatterjee et al. 2017). Since we neglect BBH mergers that occur from other formation channels, and since not every BBH may originate as a ULX, the BBH merger rates we compute could be viewed as lower limits. This is also true because we neglect mergers that originated as accreting binaries with luminosities $L_X < 10^{39}$ erg s $^{-1}$, as described at the end of Section 3. However, again, our model reproduces the inferred rate and distribution of BBH mergers from ALIGO (Abbott et al. 2016a, 2017), so that mergers from other origins are not needed. It has been suggested that the spin orbit alignment of the detected mergers make a dynamical origin for them more likely (Rodr guez et al. 2016; Abbott et al. 2017). However, a population synthesis simulation that incorporates stellar rotation indicates that an isolated binary evolution scenario can explain the ALIGO measurements (Belczynski et al. 2017). The distribution of masses observed by ALIGO (i.e., θ in Section 3.3) could be an important clue to determining whether the binary evolution of dynamic channel dominates the formation of BBH mergers. In the coming years, we will learn much about BBHs and ULXs through the detection of gravitational waves.

ACKNOWLEDGEMENTS

J.D.F. would like to thank Teddy Cheung, James Steiner, Michael Wolff, and Kent Wood for useful discussions. We are grateful to the anonymous referee for helpful comments that have improved this paper. J.D.F. was supported by the Chief of Naval Research. S.R. was partially supported by the National Research Foundation (South Africa).

APPENDIX A: METALLICITY ENHANCEMENT FACTOR

A relationship between galaxy stellar mass and metallicity was found by Tremonti et al. (2004) using a study of 53,000 galaxies at $z \sim 0.1$ from the Sloan Digital Sky Survey. Ma et al. (2016)

use cosmological simulations to derive the galaxy mass-metallicity relation and its evolution with redshift, with the simulation results matching observations at $z = 0 - 3$. We use the relationship from Ma et al. (2016), which is

$$F_{\text{OH}} = 4.45 + 0.35 \log_{10}(M_{\text{Gal}}/M_{\odot}) + 0.93 \exp(-0.43z) \quad (\text{A1})$$

where we define $F_{\text{OH}} \equiv 12 + \log_{10}(\text{O}/\text{H})$, and O/H is the average gas-phase oxygen to hydrogen number ratio in the galaxy. A study by Mapelli et al. (2010) found that the number of ULXs per star formation rate in a sample of spiral, irregular, and peculiar galaxies was anti-correlated with the galaxies’ metallicities. Taking the solar value to be $F_{\text{OH},\odot} = 8.81$, their result can be written as an enhancement factor A_{OH} in ULX formation relative to the solar value as

$$\log_{10}[A(F_{\text{OH}})] = 4.85 - 0.55F_{\text{OH}}. \quad (\text{A2})$$

The significance of this correlation was low, but at present it seems to be the best that can be done. We then define a metallicity enhancement as a function of redshift by

$$\zeta(z) \equiv \frac{\int \frac{dM_{\text{Gal}}}{M_{\text{Gal}}} \phi(M_{\text{Gal}}; z) A(F_{\text{OH}})}{\int \frac{dM_{\text{Gal}}}{M_{\text{Gal}}} \phi(M_{\text{Gal}}; z)} \times \frac{\int \frac{dM_{\text{Gal}}}{M_{\text{Gal}}} \phi(M_{\text{Gal}}; z=0)}{\int \frac{dM_{\text{Gal}}}{M_{\text{Gal}}} \phi(M_{\text{Gal}}; z=0) A(F_{\text{OH}})}, \quad (\text{A3})$$

where F_{OH} is found from M_{Gal} from Equation (A1). This function $\zeta(z)$ gives the enhancement in ULX formation per SFR at redshift z , integrated over all galaxies at that redshift, relative to the ULX production rate at $z = 0$. Here the galaxy stellar mass function as a function of z from the GOODS survey is used (Fontana et al. 2006). It is still parametrized as a Schechter function, Equation (10), but this time the parameters as a function of z are given by

$$\phi^* = 0.0035(1+z)^{-2.2} \text{ Mpc}^{-3}, \quad (\text{A4})$$

$$\log_{10}(M^*/M_{\odot}) = 11.16 + 0.17z - 0.07z^2, \quad (\text{A5})$$

$$\delta = -1.18 - 0.82z. \quad (\text{A6})$$

In Equation (A3) all integrals are performed from $10^8 M_{\odot}$ to $10^{13} M_{\odot}$, the same values used by Fontana et al. (2006) to calculate the total stellar mass as a function of z . The calculation of $\zeta(z)$ is plotted in Figure A1.

REFERENCES

- Abbott B. P. et al., 2016a, Physical Review X, 6, 041015
- Abbott B. P. et al., 2016b, Physical Review Letters, 116, 241103
- Abbott B. P. et al., 2016c, Physical Review X, 6, 041014
- Abbott B. P. et al., 2016d, ApJ, 818, L22
- Abbott B. P. et al., 2016e, Physical Review Letters, 116, 061102
- Abbott B. P. et al., 2017, Physical Review Letters, 118, 221101
- Bachetti M. et al., 2014, Nature, 514, 202
- Baldry I. K., Glazebrook K., 2003, ApJ, 593, 258
- Begelman M. C., 2001, ApJ, 551, 897
- Belczynski K., Kalogera V., Bulik T., 2002, ApJ, 572, 407
- Belczynski K., Kalogera V., Rasio F. A., Taam R. E., Zezas A., Bulik T., Maccarone T. J., Ivanova N., 2008, ApJS, 174, 223
- Belczynski K. et al., 2017, ArXiv e-prints
- Belczynski K., Repetto S., Holz D. E., O’Shaughnessy R., Bulik T., Berti E., Fryer C., Dominik M., 2016, ApJ, 819, 108

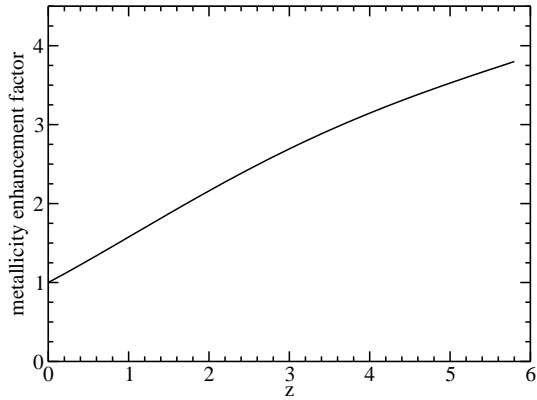


Figure A1. The metallicity enhancement factor, $\zeta(z)$.

Belczynski K., Taam R. E., Kalogera V., Rasio F. A., Bulik T., 2007, *ApJ*, 662, 504
 Bergeha C. T., Dudik R. P., Weaver K. A., Kallman T. R., 2010, *ApJ*, 708, 364
 Blecha L., Ivanova N., Kalogera V., Belczynski K., Fregeau J., Rasio F., 2006, *ApJ*, 642, 427
 Bulik T., Belczynski K., Prestwich A., 2011, *ApJ*, 730, 140
 Burgay M. et al., 2003, *Nature*, 426, 531
 Chatterjee S., Rodriguez C. L., Kalogera V., Rasio F. A., 2017, *ApJ*, 836, L26
 Colbert E. J. M., Mushotzky R. F., 1999, *ApJ*, 519, 89
 Colbert E. J. M., Ptak A. F., 2002, *ApJS*, 143, 25
 Cole S., et al., 2001, *MNRAS*, 326, 255
 de Mink S. E., Mandel I., 2016, arXiv:1603.02291
 Dominik M., Belczynski K., Fryer C., Holz D. E., Berti E., Bulik T., Mandel I., O’Shaughnessy R., 2013, *ApJ*, 779, 72
 Downing J. M. B., Benacquista M. J., Giersz M., Spurzem R., 2011, *MNRAS*, 416, 133
 Fabbiano G., 1988, *ApJ*, 330, 672
 Finke J. D., Böttcher M., 2007, *ApJ*, 667, 395
 Finke J. D., Razzaque S., Dermer C. D., 2010, *ApJ*, 712, 238
 Fontana A. et al., 2006, *A&A*, 459, 745
 Fragos T., Linden T., Kalogera V., Sklias P., 2015, *ApJ*, 802, L5
 Fürst F. et al., 2016, *ApJ*, 831, L14
 García B., Mermilliod J. C., 2001, *A&A*, 368, 122
 Georganopoulos M., Aharonian F. A., Kirk J. G., 2002, *A&A*, 388, L25
 Grimm H.-J., Gilfanov M., Sunyaev R., 2003, *MNRAS*, 339, 793
 Gris e F., Kaaret P., Pakull M. W., Motch C., 2011, *ApJ*, 734, 23
 Guti errez C. M., 2006, *ApJ*, 640, L17
 Heida M. et al., 2014, *MNRAS*, 442, 1054
 Heida M. et al., 2015, *MNRAS*, 453, 3510
 Hopkins A. M., Beacom J. F., 2006, *ApJ*, 651, 142
 Hurley J. R., Tout C. A., Pols O. R., 2002, *MNRAS*, 329, 897
 Inoue Y., Tanaka Y. T., Isobe N., 2016, *MNRAS*, 461, 4329
 Israel G. L. et al., 2017a, *Science*, 355, 817
 Israel G. L. et al., 2017b, *MNRAS*, 466, L48
 Kashi A., Soker N., 2010, *ApJ*, 723, 602
 Kewley L., Kobulnicky H. A., 2005, in *Astrophysics and Space Science Library*, Vol. 329, *Starbursts: From 30 Doradus to Lyman Break Galaxies*, de Grijs R., Gonz alez Delgado R. M., eds.,

p. 307
 Kewley L., Kobulnicky H. A., 2007, *Astrophysics and Space Science Proceedings*, 3, 435
 King A., Lasota J.-P., Kluźniak W., 2017, *MNRAS*, 468, L59
 King A. R., 2009, *MNRAS*, 393, L41
 King A. R., Davies M. B., Ward M. J., Fabbiano G., Elvis M., 2001, *ApJ*, 552, L109
 K rding E., Falcke H., Markoff S., 2002, *A&A*, 382, L13
 Kuranov A. G., Popov S. B., Postnov K. A., Volonteri M., Perna R., 2007, *MNRAS*, 377, 835
 Laycock S. G. T., Maccarone T. J., Christodoulou D. M., 2015, *MNRAS*, 452, L31
 Liu Q. Z., Mirabel I. F., 2005, *A&A*, 429, 1125
 Ma X., Hopkins P. F., Faucher-Gigu ere C.-A., Zolman N., Muratov A. L., Kere s D., Quataert E., 2016, *MNRAS*, 456, 2140
 Mandel I., de Mink S. E., 2016, *MNRAS*
 Mapelli M., Ripamonti E., Zampieri L., Colpi M., Bressan A., 2010, *MNRAS*, 408, 234
 McMillan P. J., 2011, *MNRAS*, 414, 2446
 Middleton M., King A., 2017, *ArXiv e-prints*
 Mineo S., Gilfanov M., Sunyaev R., 2012, *MNRAS*, 419, 2095
 Mizuno T., Ohnishi T., Kubota A., Makishima K., Tashiro M., 1999, *PASJ*, 51, 663
 Moffett A. J. et al., 2016, *MNRAS*, 457, 1308
 Morscher M., Pattabiraman B., Rodriguez C., Rasio F. A., Ubreit S., 2015, *ApJ*, 800, 9
 O’Leary R. M., Meiron Y., Kocsis B., 2016, *ApJ*, 824, L12
 Pakull M. W., Mirioni L., 2002, *ArXiv Astrophysics e-prints*
 Pakull M. W., Mirioni L., 2003, in *Revista Mexicana de Astronomia y Astrofisica Conference Series*, Arthur J., Henney W. J., eds., pp. 197–199
 Patruno A., Zampieri L., 2008, *MNRAS*, 386, 543
 Peters P. C., 1964, *Physical Review*, 136, 1224
 Poutanen J., Fabrika S., Valeev A. F., Sholukhova O., Greiner J., 2013, *MNRAS*, 432, 506
 Poutanen J., Lipunova G., Fabrika S., Butkevich A. G., Abolmasov P., 2007, *MNRAS*, 377, 1187
 Prestwich A. H. et al., 2007, *ApJ*, 669, L21
 Prestwich A. H., Tsantaki M., Zezas A., Jackson F., Roberts T. P., Foltz R., Linden T., Kalogera V., 2013, *ApJ*, 769, 92
 Ramsey C. J., Williams R. M., Gruendl R. A., Chen C.-H. R., Chu Y.-H., Wang Q. D., 2006, *ApJ*, 641, 241
 Ranalli P., Comastri A., Setti G., 2003, *A&A*, 399, 39
 Reynolds M. T., Miller J. M., 2013, *ApJ*, 769, 16
 Rodriguez C. L., Zevin M., Pankow C., Kalogera V., Rasio F. A., 2016, *ApJ*, 832, L2
 Sadowski A., Belczynski K., Bulik T., Ivanova N., Rasio F. A., O’Shaughnessy R., 2008, *ApJ*, 676, 1162
 Sana H., Gosset E., Naz e Y., Rauw G., Linder N., 2008, *MNRAS*, 386, 447
 S gdowski A., Narayan R., 2015, *MNRAS*, 453, 3213
 Silverman J. M., Filippenko A. V., 2008, *ApJ*, 678, L17
 Spera M., Mapelli M., Bressan A., 2015, *MNRAS*, 451, 4086
 Suh H., Hasinger G., Steinhardt C., Silverman J. D., Schramm M., 2015, *ApJ*, 815, 129
 Swartz D. A., Ghosh K. K., Tennant A. F., Wu K., 2004, *ApJS*, 154, 519
 Taylor J. H., Fowler L. A., McCulloch P. M., 1979, *Nature*, 277, 437
 Tremonti C. A. et al., 2004, *ApJ*, 613, 898
 Volonteri M., Perna R., 2005, *MNRAS*, 358, 913
 Walton D. J. et al., 2015, *ApJ*, 799, 122

Walton D. J., Roberts T. P., Mateos S., Heard V., 2011, MNRAS, 416, 1844

Wiktorowicz G., Sobolewska M., Lasota J.-P., Belczynski K., 2017, arXiv:1705.06155

Zampieri L., Roberts T. P., 2009, MNRAS, 400, 677